Dynamic brain functional connectivity analysis in migraine: a resting-state fMRI study

Cláudia Marina Alves Fonseca
claudiafonseca@tecnico.ulisboa.pt

Instituto Superior Técnico, Lisboa Portugal

October 2021

ABSTRACT

Migraine is an incapacitating neurological disorder characterised by recurring, throbbing headache attacks, generally combined with nausea, vomiting, sensory and cognitive disturbances. Migraine has become a major public health concern with a huge impact worldwide, however, its pathophysiology is not entirely understood. In order to investigate the disorder mechanisms, dynamic functional connectivity (dFC) in migraineurs was assessed through the analysis of resting-state functional magnetic resonance imaging data. Eight female menstrual episodic migraine patients without aura were scanned in the interictal (attack-free) phase of the migraine cycle, five of the eight patients in the ictal (attack) phase, and six healthy controls in the menstrual mid-cycle/post-ovulation phase to control hormonal variation in the interictal phase. To estimate the dFC, the sliding window and phase coherence methods were tested. Then, the leading eigenvector dynamic analysis focused on the dominant patterns of dFC matrices captured by leading eigenvectors, further organised into recurrent dFC states with the k-means clustering algorithm. Finally, between-group differences were statistically assessed with non-parametric permutation-based *t*-tests. Results revealed a significant increased mean lifetime and probability of occurrence in dorsal attention/frontoparietal, somatomotor and visual networks, and decreased temporal metrics in the fully connected state (global mode) in migraine patients in the ictal phase and controls compared to the interictal phase. This work reinforced the relevance of using dFC to study migraine brain, and suggested that its dysfunction might be associated with an altered dynamic of attentional/cognitive and stimulus processing systems and the global mode, which might potentially constitute neuroimaging biomarkers for disease progression.

KEYWORDS: episodic migraine, dynamic functional connectivity, resting-state functional magnetic resonance imaging, phase coherence, leading eigenvector dynamic analysis, dynamic functional connectivity states

1. INTRODUCTION

1.1. Migraine

Migraine is a complex neurological headache disorder among the most prevalent and disabling conditions worldwide, estimated to affect over 20 % of the population in a 3:1 female-to-male ratio [1]. According to the Global Burden of Disease study (2019) from the World Health Organization [2], this disorder ranks second among the world's causes of disability and first in young women [3]. Despite the massive individual impact that migraine brings, it also entails burdensome consequences on private and socioeconomic domains, especially due to the productivity losses caused by its prevalence in the youngest and most productive years of life [1][4]. Notwithstanding, migraine remains undervalued in terms of priority setting and resource allocation processes, and new therapeutics to treat this condition lack investment [5].

Migraine presents a cyclic phenotype, characterised by recurrent, incapacitating headache attacks, typically accompanied by wide-ranging symptomatology, followed by attack-free phases. A complete migraine cycle includes the interictal phase, the interval between two consecutive attacks in which the patients are usually asymptomatic, and the migraine attack, which comprises the preictal, ictal and postictal phases. Within an attack, these phases may happen sequentially, but, in most cases, they are overlapped [6].

The preictal phase, also known as the premonitory phase or prodrome, corresponds to the time before the onset of the headache and can be manifested up to 48 hours [7]. Commonly, this stage includes sensory symptoms such as photophobia, phonophobia, osmophobia, allodynia and muscular sensitivity; affective symptoms, involving irritability and depression; autonomic symptoms, namely fatigue, yawning, food cravings, thirst, flushing, sweating, nasal and sinus congestion, rhinorrhoea, frequent urination and diarrhoea; and cognitive symptoms, thought to be reversible and finished after the attack or with effective acute treatment [8]–[10]. The most common pattern of cognitive decline involves speech, reading and concentration difficulties and impaired thinking during the preictal, ictal and postictal phases, which suggests attentional and executive deficits with abnormalities in processing speed, decision-making and working memory [9][11].

Regarding the aura, this phase is experienced immediately after the prodrome, only by approximately one-third of migraineurs, and according to the ICHD-3 beta [12], it consists of a total reversible neurological disturbance and cortical dysfunction that lasts between 15 and 30 minutes [7][10]. The visual aura is the most common type of disturbance, however, other cortical perturbations may occur, involving motor, sensory and language spectra [13].

The ictal phase corresponds to the interval of 4 to 72 hours in which the patient experiences the headache and the pain severity raises to maximum. Thereafter, the postictal phase or postdrome lasts up to 24 hours after the ictal phase, being defined as the period between the resolution of the headache and total recovery. Despite the large neglection of this phase by the scientific community, which is not even documented in the ICHD-3 beta [12], migraineurs report symptoms after the headache involving tiredness, attention deficits and neck stiffness [14][15].

Although the interictal phase of the migraine cycle is tendentially asymptomatic, converging evidence points to the existence of an habituation response deficit in this period of the cycle. Instead of a regular habituation effect, with a "response decrement" resulting from the exposure to repeated stimuli, interictal migraineurs exhibit an initial weaker response that intensifies with persistent stimulation, leading to some vulnerability in those conditions (e.g. exposure to sensory inputs) [11]. Hence, the peculiarities of each phase and the intra- and inter-patient varying symptoms contribute to the huge complexity of this disorder.

The origin of migraine attacks and the underlying brain structures and neurobiological processes involved in their progression remains unclear and under clinical and scientific research. Currently, the putative basis for migraine attacks is the activation of the meningeal nociceptors and, consequently, the trigeminovascular (TV) system, followed by its peripheral and central sensitisation. The activation of the meningeal nociceptors due to the neurogenic inflammation [8] activates the TV neurons in the spinal trigeminal nucleus, together with incoming signals from the head and neck. These signals ascend through the quintothalamic tract to the brainstem and high cervical spinal cord, which participate in the processing of the nociceptive signals, synapsing with the thalamic neurons [16]. Thereafter, the thalamus transmits nociceptive inputs to the cortex, especially to the primary and secondary somatosensory cortices and insula, and the somatosensory and visceral inputs project from the head and orofacial regions to the hypothalamus, through the trigeminohypothalamic tract [17]. The perception and modulation of nociceptive information are affected by a set of pain-modulatory circuits that involve the brainstem, thalamus, hypothalamus and cortex [17].

1.2. Resting-state fMRI and functional connectivity

In the last two decades, technologies to investigate migraine pathophysiology progressed greatly. Neuroimaging techniques, particularly Blood Oxygen Level Dependent-functional magnetic resonance imaging (BOLD-fMRI), have become an indispensable tool in migraine research and have driven robust advances in understanding migraine generation, progression, chronification and treatment [18].

Resting-state fMRI (rs-fMRI), which focuses on the spontaneous low-frequency fluctuations of the BOLD signal by scanning patients at "rest" (with the absence of any imposed task), has gained widespread acceptance in the neuroscience community as a powerful technique to explore spontaneous brain activity and functional connectivity (FC) for characterising brain's spatiotemporal organisation and mapping brain function [19]. FC can be defined as the coherence (or statistical temporal dependence) between BOLD signal fluctuations [20],

The FC analysis in rs-fMRI studies has been widely explored. Over the years, resting-state networks (RSNs) composed of regions with low-frequency synchronous fluctuations have been identified, contributing to study brain's functional architecture [21]. Templates of well-established RSNs commonly used as reference are the Yeo repertoire [22], which comprises seven RSNs – visual (VN), somatomotor (SMN), ventral attention (VAN), dorsal attention (DAN), limbic (LN), frontoparietal (FPN) and default mode (DMN) networks – and Smith's template, with ten RSNs – visual medial, occipital and lateral (VMedN, VOccN, VLatN), right and left FPN, DMN, SMN, auditory (AudN), executive control (ECN) and cerebellar (CbN) networks.

Most FC studies assume connectivity stationarity over the full rs-fMRI scan (static FC or sFC). Notwithstanding, the prior assumption that FC did not fluctuate over time started to be interpreted as too simplistic to capture the full extent of resting-state activity [23]. Hence, in the 2000s, studies suggesting the dynamic behaviour of FC on short-time scales started to arise, namely throughout ageing, development and visual state. Throughout the years, the limitations of sFC analysis and improvements in recording methods shifted the attention to the concept of dynamic FC (dFC), allowing the detection of time-varying patterns of neuronal connectivity and the appearance of quasi-stable recurrent FC states that resemble brain networks [23].

Up to now, two main methods have been used to estimate the dFC: the sliding window (SW) Pearson correlation and the phase coherence (PC) methods. The SW segments fMRI data in successive intervals of time (temporal windows), within which the FC is described between each pair of brain regions by computing a pairwise (typically Pearson) correlation between their respective BOLD signal time courses [24]. For a sliding window with length *W,* the dFC between two brain regions *n* and *p* at each time point *t* can be given by the Eq. (1.1):

$$dFC(n,p,t) = corr({x_{n,t}}^{t+W-1}, {x_{p,t}}^{t+W-1}) \quad (1.1)$$

where *corr()* is the FC metric of interest, and ${\mathrm{x}_{\mathrm{n},t}}^{t+W-1}$ and ${\mathrm{x}_{\mathrm{p},t}}^{t+W-1}$ are the BOLD time courses of the brain regions *n* and *p*, respectively, segmented in time from *t* to *t* + *W* - 1 [23]. The SW approach provides a robust pipeline to obtain FC estimates and is less susceptible to noise than other techniques such as PC. However, it compromises the temporal resolution of the data, precluding the detection of FC patterns with durations below the window size [23][25].

To overcome these caveats, the PC method characterises the time-varying single frame FC by converting each BOLD time course into its complex analytic version (instantaneous amplitude and phase) with the Hilbert transform [26], and then comparing instantaneous phase information between BOLD signals of different brain regions. The degree of phase synchronisation between brain regions *n* and *p* at time point *t*, also called phase coherence, measures the dFC [27], as described in Eq. (1.2):

$$dFC(n,p,t) = cos\,[\theta(n,t) - \theta(p,t)] \quad (1.2)$$

where $\theta(n,t)$ and $\theta(p,t)$ are the instantaneous phases of regions *n* and *p*, respectively, at the time point *t.* The implementation of the PC method has been an emerging tool in fMRI due to its great advantages, namely the ability to characterise the dFC at each repetition time (TR), ensuring a maximum temporal resolution and a more accurate analysis of the faster dFC fluctuations. Furthermore, since this metric is applied instantaneously for each time point and the whole brain with one transform, it is computationally faster than temporal correlations. Also, since PC is a non-linear measure, it is more suitable to detect complex dynamic processes in the brain [27].

In particular, a method implemented by Cabral et al. [26], the leading eigenvector dynamic analysis (LEiDA), has proposed to represent the PC between brain regions using the largest magnitude eigenvector of BOLD phases (*N* elements per time), which explains over 50% of data variance, instead of the whole *N*×*N* phase synchronisation matrix. The LEiDA allows to reduce data dimensionality, improve cluster performance, and detect recurrent BOLD phase patterns that closely overlap with previously defined RSNs [28].

Over the past years, much progress has been made in migraine neuroimaging research and study of FC, providing new insights regarding the alterations in migraine brain FC throughout the migraine cycle and compared to healthy subjects [29]. Hence, the present work proposes to investigate for specific dFC alterations in migraine, by comparing episodic migraine patients without aura in the interictal and ictal phases of the migraine cycle, and migraineurs with healthy controls (HC), evaluate its relation with migraine mechanisms and, potentially, identify neuroimaging biomarkers to track disease progression and response to treatment.

2. METHODS

2.1. Data description

2.1.1. Participants

rs-fMRI imaging data used in the present work was gathered in the scope of the *MIG_N2Treat* project, at Hospital da Luz, with data collected from October 2019. The participants of this project were 8 female patients with menstrual and menstrually-related episodic migraine without aura and 6 HC. Regarding migraineurs, the exclusion criteria were the following: previous history of migraine with aura or chronic migraine; presence of another type of headache, neurological disorder or psyquiatric disorder; taking any drugs affecting the central nervous system; being under phophylactic treatment; daily alcohol or tabacco consumption; and non-compatibility with MRI.

All migraine patients underwent the rs-fMRI scan in the interictal phase of the migraine cycle, whereas just 5 of the 8 were scanned in the ictal phase. The HC were scanned in the mid-cycle/post-ovulation phase of the menstrual cycle to control for hormonal variation in the interictal phase of the migraine cycle. The ages of the participants ranged between 21 and 45 (34.1 ± 9.0) years old for the migraine group and between 22 and 39 (27.7 ± 6.0) years old for the HC.

Within the migraine ictal group, clinical features regarding the ongoing attack were registered and averaged across the 5 patients: attack frequency per month of 3.9 ± 2.0; usual attack duration of (41.6 ± 23.0) hours; mean pain intensity of the attack in a mild (1)-to-severe (3) scale of 2.6 ± 0.5 and in the Visual Analogue Scale (0-10) of (6.2 ± 0.7) hours. Furthermore, regarding migraine-associated symptoms, ictal patients were interrogated with a yes (1)-or-no (0) question and the answers were averaged across participants: 1.0 for nausea; 0.4 ± 0.5 for vomit; 0.8 ± 0.4 for photophobia; 1.0 for phonophobia; and 1.0 for motion sensitivity.

2.1.2. Image acquisition protocol

Regarding the image acquisition, structural and functional data were acquired on a 3 Tesla Siemens MRI system. The structural scans were collected with a T_1-weighted magnetization-prepared rapid gradient echo (MPRAGE) series, with TR = 2300 ms, time echo (TE) = 2.98 ms and 1 mm isotropic resolution. The rs-BOLD fMRI scans were acquired for 7 minutes using a T_2*-weighted gradient-echo 2D-EPI sequence, with TR = 1260 ms, TE = 30 ms and 2.2 mm isotropic resolution. In the rs-fMRI scans, 333 volumes were acquired, each consisting of 60 axial slices of the whole brain, with an SMS acceleration factor of 3 (*z* direction) and a generalized autocalibrating partial parallel acquisition (GRAPPA) acceleration factor of 2 (*y* or phase encoding direction). During the rs-scan, participants were asked to stay motionless with eyes open and without falling asleep.

2.2. rs-fMRI data preprocessing and parcellation

The rs-fMRI data analysed in this work were preprocessed by the team using the *FMRIB's Software Library® (FSL)* and the *MATLAB 2016b Software® (The Math-Works Inc., Natick, MA, USA)*.

The preprocessing steps were the following: **(i)** brain extraction to remove the skull, and other non-brain tissues [30]; **(ii)** segmentation and bias field correction [31], with the creation of white matter (WM) and cerebrospinal fluid (CSF) masks further binarized in the structural space; **(iii)** motion correction, which included the estimation of the 6 motion parameters (3 translations and 3 rotations) for each volume with respect to the middle one [32], application of a rigid body (RB) geometrical transformation based on the motion parameters, and alignment of volumes to the reference; **(iv)** EPI distortion correction (unwarping); **(v)** registration, which comprised the alignment of the subject's functional and structural images (linear RB transformation

with 6 degrees of freedom) and the registration from the structural to the 2 mm MNI152 standard space (non-linear transformation) [33], and the registration of the WM and CSF masks into the functional space, eroded with a spherical Gaussian kernel of 2.2 mm and 1.8 mm radius, respectively; **(vi)** semi-automatic classification of ICA components into the signal of interest or noise and ICA noise clean-up to regress the noise components out of the original fMRI data [34][35]; **(vii)** nuisance regression to regress the nuisance time series out of the data (6 RB motion parameters, motion outliers, and average WM and CSF signal), which entered into a GLM fitted to the data [36]; **(viii)** high-pass filtering with a cut-off period of 100 s [36]; **(ix)** spatial smoothing with a full width at half maximum of 3.3 mm (1.5 times the voxel size) [19][37].

After preprocessing, the rs-fMRI data were parcellated using four commonly used atlases: AAL with 90 cortical and subcortical ROIs (AAL90) [38]; AAL with 116 cortical, subcortical and cerebellar ROIs (AAL116) [38]; Desikan with 66 cortical ROIs [39]; and Harvard-Oxford with 63 cortical and subcortical ROIs. The following processing steps were performed using the *MATLAB 2016b® software,* and the LEiDA was applied following Cabral et al.'s pipeline [40].

2.3. rs-fMRI data processing

2.3.1. dFC estimation

The estimation of the dFC was performed using two different approaches: the SW and the PC. The first step for both methods consisted of filtering the preprocessed ROI-averaged BOLD signal in the low-frequency range of 0.01 Hz to 0.1 Hz (meaningful frequencies of resting-state fluctuations) using a second-order Butterworth band-pass filter (**Fig. 1.A.**) [20][41].

To implement the SW analysis, three window sizes were tested – 25 TR (corresponding to 31.5 s), 35 TR (44.1 s) and 45 TR (56.7 s), slid in steps of 1 TR (1.26 s). According to the literature, window sizes in the range of 30 s to 60 s are a reasonable choice to capture dFC patterns, and steps of 1 TR are commonly used [42]. Thereafter, the Pearson correlation coefficient was computed within each window for all pairs of filtered ROI-averaged BOLD signal time courses (Eq. (1.1)), yielding an $N \times N$ symmetric dFC matrix per window (time) and subject, in which N stands for the number of brain regions of the atlas.

The PC analysis was performed with the Hilbert transform approach. The instantaneous phase was extracted from the filtered ROI-averaged BOLD signals (**Fig. 1.B.**), and the dFC was obtained by computing the phase synchronisation of for all pairs of ROIs (Eq. (1.2)), originating an $N \times N$ symmetric dFC matrix per TR and subject, capturing the BOLD PC throughout the whole brain over time. This matrix is illustrated in **Fig. 1.C.**, with the colours ranging from red (full synchrony of BOLD phases) to blue (phase difference of 180º).

2.3.1.1. Comparison of dFC matrices

To evaluate the degree of similarity between the dFC matrices obtained with both methods, the cosine similarity coefficient was used. The literature suggests that this metric provides better results than the Pearson correlation [40]. Thus, the dFC matrices obtained per TR with the PC (higher temporal resolution) were averaged within each window used in the SW approach. Then, the cosine similarity coefficient ($CS_{SW,PC}$) was computed between the *N×(N-1)/2* upper triangular elements (concatenated into a vector) of the dFC matrices obtained with the SW (x_{SW}) and the averaged ones obtained with the PC (x_{PC}). The expression is described in Eq. (2.1):

$$CS_{SW,PC} = \frac{x_{SW} \cdot x_{PC}}{\|x_{SW}\| \|x_{PC}\|} \qquad (2.1)$$

where$\| \ \|$ is the Euclidean norm. The cosine similarity is equal to 1 for maximal similarity and -1 for maximal dissimilarity.

2.3.2. LEiDA

After estimating the connectivity time courses, following Cabral et al.'s pipeline [40], the LEiDA was implemented into the dFC matrices yielded by PC and SW, since the leading eigenvectors were able to explain the majority of the dFC variance in both metrics. Regarding the PC method, V_1 describes the main orientation of BOLD signal phases across the N brain regions over time, and each element of V_1 represents the projection of the BOLD phase of the given brain region into this leading eigenvector (**Fig. 1.D.**). If all elements of V_1 have the same sign, then all BOLD phases are pointing in the same direction and following the main orientation determined by V_1 (strong coherence), also called the global mode of BOLD signal fluctuation. Instead, if BOLD signals have different orientations with respect to V_1 (positive and negative signs), the brain can be divided into two communities according to the BOLD phase relationships between the brain regions. The magnitude of each element of V_1 represents the strength with which brain regions belong to those communities [43]. The present work used the convention that the global mode is characterized by positive values of V_1 across all brain regions, so detachments from the global mode are represented by negative values.

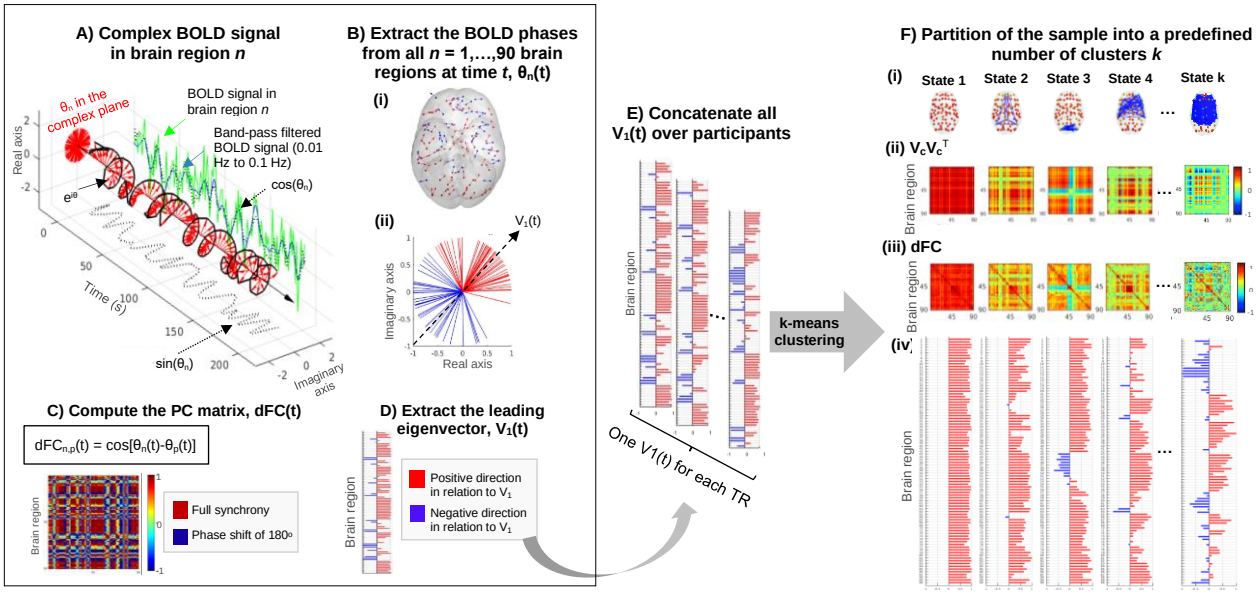

Fig. 1. Pipeline of LEiDA, with the AAL90 atlas (parcellation scheme) and PC method (estimation of dFC). **A)** The BOLD signal in a given brain region *n* (green) is band-pass filtered (blue) and Hilbert transformed into a complex analytic signal. The signal phase is represented by $e^{i\theta}$ across time *t* (black line) and at each TR (red arrows), where the real part is given by $cos(\theta_n)$ and the imaginary part by $sin(\theta_n)$. **B)** BOLD phases of all brain regions represented in **(i)** cortical space, with arrows centered at the center of gravity of each ROI and **(ii)** in the complex plane, with phases centered in the origin of a unit circle with real and imaginary axis. **C)** PC matrix (dFC(t)). **D)** Leading eigenvector of the dFC matrix ($V_1(t)$). **E)** Concatenation of $V_1(t)$ over time and across subjects and partition into *k* clusters or dFC states. **F)** dFC states displayed according to their decreasing probability of occurrence and represented by the respective V_c: **(i)** as a network in the AAL90 cortical space (axial slice), in which the elements of V_c are placed at the center of gravity of the respective brain region, shaped as spheres colored according to their sign (red to yellow spheres represent positive elements from 1 to 0, cyan to dark blue represent negative elements from 0 to -1), and areas with $V_c \leq 0.1$ are linked with blue edges; **(ii)** by the outer product $V_cV_c^T$, that represents a N×N connectivity pattern where each $V_c(n)$ weights the contribution of each brain region n to that pattern; and **(iv)** as a bar plot displaying the projection of the BOLD phase in each brain region into V_c. dFC states are also characterised by their **(iii)** dFC matrix.

2.3.3. dFC states

To identify recurrent FC patterns, the k-means clustering algorithm was implemented at a group-level in the migraine interictal dataset (8 subjects, total of 8 samples); in a group composed of the interictal and ictal dataset (5 subjects in the interictal and ictal phases, total of 10 samples); and in a group including the interictal and HC dataset (6 subjects in the interictal phase and 6 HC, total of 12 samples).

This factorisation technique received as input the leading eigenvectors estimated from the dFC matrices concatenated over time and subjects (**Fig. 1.E.**) and was run with *k* ranging from 3 to 15 (i.e., dividing the total number of leading eigenvectors into 3 to 15 clusters) to cover the range of functional networks that is commonly found in the literature [28][43]. Moreover, the cosine distance was chosen as the distance metric for minimization since it gave more meaningful results than the squared euclidean distance (higher specificity in detecting well-established RSNs). To increase the likelihood of escaping local minima and ensure consistency in the results, the k-means clustering algorithm was run 1000 times, and the best result that minimized the distance between the cluster point and its centroid was selected.

After implementing this method, the leading eigenvectors were reorganised into a predefined *k* number of clusters or dFC states representing recurrent patterns of BOLD phase coherence (**Fig. 1.F.**). Each FC pattern was described through its *N×1* cluster centroid vector V_c (c = 1 to k) in three different ways. **(i)** In cortical space. Areas with $V_c \leq 0.1$ are linked with blue edges to represent the network created by the smallest community of brain regions. Several thresholds for the links were tested, though, this value allowed for better specificity in the network detection; **(ii)** Back into matrix format, through the outer product of V_c with V_c^T. This yields an *N×N* connectivity pattern with each element weighting the contribution of each brain region to that pattern. Positive red values are set to pairs of brain regions with the same sign of V_c (coherent BOLD signals) and negative blue values to pair of areas with different signs of V_c; **(iv)** And as a bar plot, showing the projection of the BOLD phase of each brain region into V_c. Also, dFC states were represented by its **(iii)** *N×N* dFC matrix, corresponding to the average of the dFC matrix over the time points in which the respective state occurred [40][43].

After estimating the dFC states, they were characterised using predefined temporal metrics: the mean lifetime (or dwell time), which corresponds to the mean number of consecutive epochs in the given state; the probability of occurrence (or fractional occupancy), which is the fraction of epochs the state occurred throughout the scan; and the switching profile, which summarises the probabilities of switching from a given dFC state to another [40].

2.3.4. Statistical analysis

2.3.4.1. Correlation of dFC states with RSNs

While RSNs consist of temporal patterns that replicate across space, dFC states represent spatial patterns that replicate over time [40]. Nevertheless, the latter are expected to reveal sub-parts of specific RSNs, combinations of different RSNs or even resemble entire RSNs. In order to assess the correspondence of the obtained dFC states with well-established RSNs reported in the literature, the correlation of the cluster centroid vectors with the vetors corresponding to the RSNs in atlases spaces was computed, following the same method used by Cabral and colleagues [40].

Firstly, the seven Yeo RSNs defined in 2 mm^3 MNI space by Yeo and colleagues [22] were transformed into the atlas (AAL90, AAL116, Desikan and Harvard-Oxford) space. This process yielded a matrix with size *N* ROIs × 7 RSNs, i.e., seven vectors with as many elements as the number of ROIs of the given atlas, where each element corresponds to the voxels in each brain area belonging to the corresponding Yeo network. Since the network contrasting from the global mode in each state is represented by elements with a negative sign in the respective element of V_c, the RSNs vectors were transformed to their symmetric, so that they could be compared with the V_c's. Moreover, since the global mode does not define a functional network of BOLD signal decoupling, the correlation with RSNs was not computed for this state. This sequence of steps was also applied to the ten RSNs defined by Smith and colleagues in 2 mm^3 MNI space [44].

After this transformation, the Pearson correlation coefficient was computed between the cluster centroid vectors of the dFC states corresponding to the partition model being studied and the transformed RSNs vectors. For all partition models studied with the k-means clustering, *k* hypotheses were tested for each FC repertoire. Therefore, to correct for multiple comparisons, the standard significance threshold 0.05 was adjusted with a Bonferroni correction to 0.05/*k*, and the statistically significant correlations were those with the respective *p*-values inferior to that threshold [43].

2.3.4.2. Comparison between groups

In order to statistically assess between-group significant differences in terms of the temporal metrics (mean lifetime and probability of occurrence) of the obtained dFC states, non-parametric permutation-based *t*-tests with 10,000 permutations were implemented on these two metrics. In the results obtained with the group composed of the migraine patients scanned in the interictal and ictal phases, a permutation-based paired *t*-test was implemented, since it compared paired observations of the same subject in two different conditions. Instead, in the results obtained with the group including migraineurs in the interictal phase and HC, a permutation-based unpaired *t*-test was applied, since it compared two unrelated and independent groups [45]. Afterwards, the results were analysed by plotting the *p*-values for the whole FC repertoire over the range of *k*s. The significance of the results was evaluated using as reference three thresholds for the *p*-values: the standard significance threshold, 0.05; the Bonferroni corrected significance threshold, 0.05/*k*, to correct for multiple comparisons by considering the number of states (independent hypotheses) compared within each partition model; and the corrected significance threshold, 0.05/Σ*k*, to correct for multiple comparisons by considering all hypothesis independent across models, including the whole sample of tests performed [43].

3. RESULTS AND DISCUSSION

3.1. Comparison between dFC matrices: SW vs. PC methods

In order to compare the dFC matrices estimated for the AAL90, AAL116, Desikan and Harvard-Oxford atlases with the SW and PC methods in the interictal dataset, the cosine similarity was computed between the dFC matrices obtained with the SW and the averaged ones obtained with PC within the respective window (sizes of 25 TR, 35 TR and 45 TR and step of 1 TR). The results are depicted in **Fig. 2.**

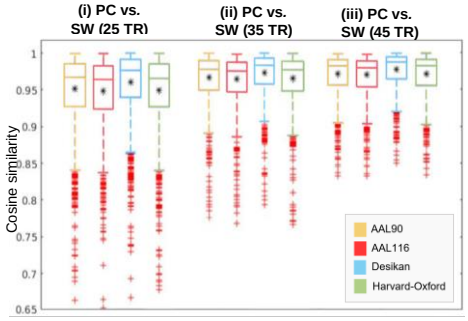

Fig. 2. Cosine similarity values computed between the dFC matrices obtained with the SW and the averaged ones obtained with PC within the respective window (**(i)** size of 25 TR, **(ii)** 35 TR and **(iii)** 45 TR, all slid in steps of 1 TR), for the four atlases in the interictal group. The median is represented by the horizontal line within the box plot, the mean value is denoted with a black asterisk (∗) and the outliers are marked with the red plus (+).

By looking at the box plots, it is possible to observe that, regardless of the brain parcellation scheme and the window size chosen for the SW, the cosine similarity values are always above 0.650, the medians above 0.960 and the means above 0.940. Furthermore, it was found that the distribution of data points tends to narrow for larger window sizes (fewer outliers with lower cosine similarity values), resulting in a slight increase in the medians and means. This observation might be associated with the fact that larger window sizes lead to the inclusion of more data points in the average of the PC dFC matrices within the window and, consequently, to the increase of the SNR, which would explain a slightly higher similarity between the dFC matrices obtained with the PC and SW with a size of 45 TR.

Thus, despite the methodological differences between the SW and PC, these results suggest that the connectivity information they provide is overall similar.

3.2. Analysis of migraine interictal dataset

After extracting the leading eigenvectors of the dFC matrices estimated with both methods, the k-means clustering algorithm was implemented in the migraine interictal group with the predefined number of clusters ranging from k = 3 to k = 15. In the following section,

the AAL90 atlas was chosen as the reference brain parcellation scheme, since it is the most commonly used in literature [26][28][40].

3.2.1. Comparison between SW and PC methods

To evaluate how dFC states varied between methods, the k-means clustering algorithm with k = 5 was run for PC and SWs of 25 TR, 35 TR and 45 TR, with the AAL90 atlas. This partition model was chosen since it has been used in several studies as the best clustering solution to represent FC data [24][40] and provides a low set of synchronisation patterns, facilitating the following analyses. The axial cortical representation of the obtained dFC states is depicted in **Fig. 3.**

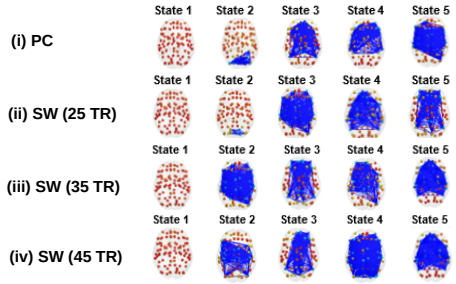

Fig. 3. dFC states obtained with the k-means clustering algorithm (k = 5), displayed according to their decreasing probability of occurrence, for the AAL90 atlas, **(i)** PC and SW of **(ii)** 25 TR, **(iii)** 35 TR, **(iv)** 45 TR methods.

For all clustering solutions depicted in **Fig. 3.**, state 1 (most prevalent state) is consistent and exhibits all brain regions with BOLD phases aligned with each other and projected toward the same direction into the leading eigenvector (i.e., only positive red elements in the cluster centroid vector), and does not show the separation of any particular subsystem nor a significant correlation with RSNs of reference, being called the global mode. This state is extensively reported in the literature [24][40]. From the second state on, small groups of brain regions exhibit BOLD phases that deviate from the global coherence state and start to form functional networks (areas with $V_c \leq 0.1$ linked by the dark blue edges).

Although the average dFC matrices yielded by PC method presented a high degree of similarity with those yielded by SW (**Fig. 2.**), results obtained with the k-means clustering algorithm for k = 5 reveal that the dFC states differ greatly between both methods.

By qualitative analysis of **Fig. 3.**, the FC patterns identified with the PC seem to be more consistent with those obtained with the SW of 25 TR, showing notable deviations compared to the results of SWs with larger sizes (35 TR and 45 TR) that present more irregular states. In particular, the occipital state, which is extensively reported in the PC literature [40][46], can be identified in the results obtained with the SW of 25 TR (although with less pronunciation than in PC) but it does not appear for the wider SWs.

3.2.1.1. Correlation between cluster centroid vectors

To quantitatively understand the similarities between the dFC states obtained with different methods, the Pearson correlation coefficient was computed for each pair of cluster centroid vectors (excluding the global mode) obtained with the PC and SW methods for the partition model k =5) (**Fig. 4.**).

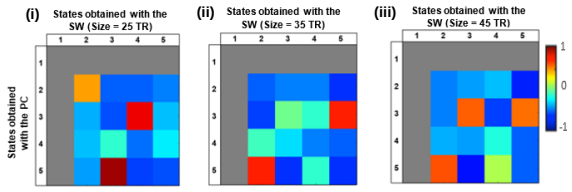

Fig. 4. Pearson correlation coefficient computed between the cluster centroid vectors of the dFC states obtained with the PC and SW of **(i)** 25 TR, **(ii)** 35 TR, **(iii)** 45 TR methods. The global mode was not evaluated.

By analysing the correlation matrices, it was not found any univocal correlation between states of different methods. However, results from **Fig. 4. (i)** reveal that the centroid vectors of state 2, state 3 and state 5 obtained with PC and those of state 2, state 4 and state 3 identified with the SW of 25 TR are, respectively, meaningfully correlated. For the dFC states yielded by larger SWs, the number of correlated states increases, such that a single state from the PC FC repertoire presents multiple meaningful correlations with states yielded by SW (e.g., in **Fig. 4. (iii)**, the state 3 obtained with the PC is greatly correlated with state 3 and state 5 yielded by SW of 45 TR). This suggests that, contrarily to the PC, the functional subsystems identified with the SW start to appear intermingled within each cluster, such that the correlation departs from univocity. Furthermore, results show that the wider the window, the lower the correlation with the centroid vectors obtained with the PC (the maximum r in **Fig. 4. (i)**, **(ii)** and **(iii)** is 0.95, 0.75 and 0.69, respectively). Hence, this quantitative analysis reinforces the higher degree of similarity between the repertoire obtained with the PC and the SW of 25 TR, and the divergence of results for larger windows, as expected. In fact, although the connectivity time courses yielded by PC and SW of 45 TR display slightly higher similarity (**Fig. 2.**), smaller SWs produce dynamic analyses on closer temporal scales (or resolution), and therefore yield more similar dFC states.

3.2.1.2. Correlation of dFC states with RSNs

Next, in order to quantitatively assess the influence of using the PC or SW in the reliability of the results, the dFC states obtained with both methods were compared with well-established RSNs, by computing the Pearson correlation coefficient between the cluster centroid vectors of the dFC states for k = 5 and the seven Yeo transformed RSNs vectors.

Results reveal that the FC patterns obtained with the PC present statistically significant correlations with the VN (r = 0.80, p-value = = $2.27 * 10^{-21}$), SMN (r = 0.73, p-value = $5.27 * 10^{-16}$), VAN (r = 0.58, p-value = $1.53 * 10^{-9}$) and DMN (r = 0.28, p-value = $7.40 * 10^{-3}$) in distinct clusters. In the SW of 25 TR, the VN is also detected separately in state 2, although it does not correlate significantly with any Yeo RSN. Regarding the remaining SWs, the VN arises in the state 5 obtained with the SW of 35 TR (r = -0.31, p-value = $2.80 * 10^{-3}$) and 45 TR (r = -0.32, p-value = $2.10 * 10^{-3}$), though, it is not detected separately, as it appears intermingled with the DMN with lower correlation coefficients (absolute value) and statistical significance (r = 0.38, p-value = $2.29 * 10^{-4}$ for the SW of 35 TR and r = 0.34, p-value = $1.00 * 10^{-3}$ for a size of 45 TR). In the SW of 25 TR, the DMN arises separately in state 4 (r = 0.34, p-value = $9.10 * 10^{-4}$). Regarding the SMN, it appears for the three SWs (r = 0.66, p-value = $1.02 * 10^{-12}$ for the SW of 25 TR, (r = 0.42, p-value = $3.76 * 10^{-5}$ for a size of 35 TR, and r = 0.52, p-value = $1.89 * 10^{-7}$ for a size of 45 TR). In contrast to the PC method, none of the SWs can detect the VAN. However, in the results obtained with the window of 45 TR, the DAN arises in state 4 (r = 0.41, p-value = = $6.36 * 10^{-5}$). This network does not correlate with any dFC state obtained with the PC.

Therefore, results suggest that the recurrent states obtained with the PC method are more similar to the functional networks of reference VN and SMN than those obtained with the SW method (higher correlation coefficients) and present stronger statistical significance, i.e., lower p-values. Furthermore, excluding the global mode, while each of the four dFC states obtained with the PC method presents a statistically significant correlation to one network of reference (in total, four Yeo RSNs are detected), states obtained with the SWs of 25 TR, 35 TR, and 45 TR significantly correlate with a total of two, three, and four Yeo RSNs, respectively. These observations show that, for the shortest window size, just half of the Yeo RSNs is significantly detected compared to the PC results, and for larger window sizes, the overlap with the Yeo RSNs increases, but they start to appear intermingled within each state. Thus, we may speculate that the PC is more sensitive than SW in detecting RSNs, presumably due to the inherently higher temporal resolution.

In fact, whereas the PC method allows for a maximal temporal resolution, estimating the instantaneous synchronisation of BOLD phases (one connectivity matrix per TR), the SW describes statistical relationships between brain regions within successive fixed-length windows (25 TR, 35 TR and 45 TR, in this case). Thus, the concept underlying the SW method implies focusing on the lower frequencies of the data (introduction of 31.5 s, 44.1 s and 56.7 s of period, respectively), which worsens the temporal resolution and may affect the detection of recurrent FC patterns with shorter mean lifetimes (i.e., that occur more rapidly). It should also be noted that the percentage of variance explained by the leading eigenvector was not above 50% for all data points in the SW, which may have led to a misleading representation of the FC dominant pattern by the leading eigenvectors in some cases, and affected the representation of dFC states.

Therefore, although the PC presents more susceptibility to noise than the SW, results suggest that the first method is more suitable to assess faster fluctuations of dFC, since it captures a dynamic that effectively exists and is not purely noise (otherwise the SW would probably detect it more reliably). This conclusion was also presented

by Cabral and colleagues [24], which suggested the existence of a fast dynamic of functional FC patterns evolving, at least, at the temporal resolution of acquisition (in this case, corresponding to TR = 1.26 s), which would only be detected by keeping the high frequency components of the BOLD signal.

3.2.1.3. Dynamics of FC states

In order to compare the temporal metrics of the dFC states obtained with the PC and SW methods, the mean lifetime and probability of occurrence of each synchronisation pattern are displayed in **Fig. 5.** for the partition model k = 5.

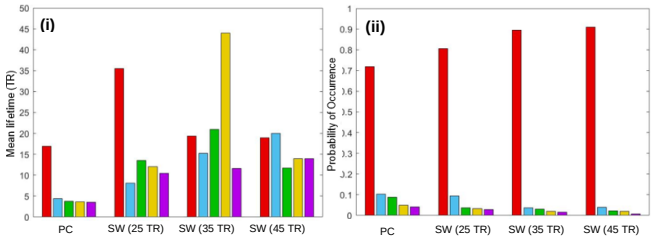

Fig. 5. Mean lifetime (**i**) and probability of occurrence (**ii**) of each dFC state (k = 5) obtained for the PC and SW of 25 TR, 35 TR and 45 TR.

By comparing the temporal metrics between the PC and SW methods (**Fig. 5. (i)**), it was found that the mean lifetimes of the dFC states are higher in the SW. Within the SW method, since the duration of the states tends to increase for wider window sizes, the mean lifetime of the global mode decreases, approximating the duration of the remaining patterns. Indeed, as described in the previous section, the SW method focuses on the lower frequency components of the BOLD signal. This method introduces by itself a temporal smoothing during the estimation of the FC within successive intervals of time, which increases the period of fluctuations and the mean lifetimes of the dFC states. Thus, synchronisation patterns with mean lifetimes shorter than the window size are hardly detected by this method. Following the same reasoning, wider window sizes (stricter low-pass filter) are expected to originate dFC states with higher mean life-times on average, which is also observed (except for the SW of 45 TR).

The findings above do not clarify whether the FC patterns present short mean lifetimes that appear longer in the SW because the method extends their duration over time and excludes shorter instances, or if the states have, in fact, high mean lifetimes, being better detected by filtering the high frequencies of the signal. Nonetheless, the correlation with the Yeo repertoire analysed in the previous section shows the importance of a fine-grained temporal specificity in detecting functional networks, and Cabral et al. [24] emphasize the relevance of keeping the higher frequencies of the BOLD signal to detect the fast evolution of dFC at a scale at least as fast as the acquisition TR. These observations point to the ability of the PC method to capture a fast functional dynamic that exists and approximates the dynamic of the rs-fMRI (0.01 Hz to 0.1 Hz), which can not be reproduced with the SW method.

Furthermore, **Fig. 5. (ii)** reveals that the global coherence state tends to be more prevalent (higher probability of occurrence) and occur in shorter continuous time periods (lower mean lifetime) for the SW method than the PC method. As expected, the higher the probability of occurrence of the global mode, the lower the probabilities of the remaining FC patterns, which is visually detected in the same figure.

3.3. Comparison between groups

3.3.1. Migraineurs: Interictal vs. Ictal

Migraine interictal and ictal sessions were compared by implementing a permutation-based paired t-test on the mean lifetime and probability of occurrence of the dFC states. Then, the FC patterns with statistically significant between-session differences on those temporal metrics were analysed. The *p-values* associated with the solutions obtained for the whole FC repertoire studied (k = 3 to k = 15) with the AAL90 atlas and PC method are displayed in **Fig. 6.**, although this analysis was also performed for the remaining atlases (AAL116, Desikan and Harvard-Oxford). The red dashed line represents the standard significance threshold, p-value = 0.05; the green dashed line corresponds to the Bonferroni corrected significance threshold to correct for multiple comparisons by considering the number of states (independent hypotheses) compared within each partition model, p-value = 0.05/k; and the blue dashed line represents the corrected significance threshold to correct for multiple comparisons by considering all hypothesis independent across models, including the whole sample of tests performed, p-value = 0.05/Σk [43].

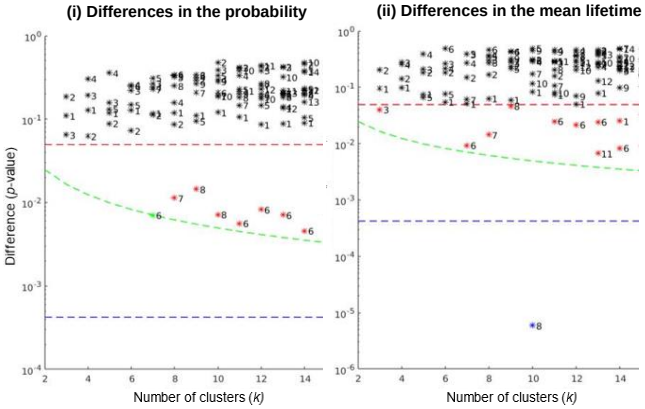

Fig. 6. Significance of between-session differences in the **(i)** probability of occurrence and **(ii)** mean lifetime of each dFC state, obtained with the AAL90 atlas and PC method, between migraine interictal and ictal sessions, as a function of k.

Of the clustering solutions considered, most dFC states did not present any significant difference between the interictal and ictal sessions (black asterisks). Moreover, several solutions obtained for the probability of occurrence and mean lifetime were revealed to be possible false positives (red asterisks). Only two solutions survived the correction for multiple comparisons: state 6 for k = 7 (green asterisk, p-value < 0.05/k) and state 8 for k = 10 (blue asterisk, p-value < 0.05/Σk), with significant between-session differences in the probability of occurrence and mean lifetime, respectively.

For the subsequent analyses, the partition model with the lowest k and, simultaneously, with the solution displaying the p-value below the most significant threshold will be studied. For example, the chosen partition model for this atlas will be k = 10, since it is the shortest repertoire displaying a solution below the most significant threshold (p-value < 0.05/Σk). Moreover, states with significant between-session differences in temporal metrics will also be analysed in in terms of FC strength or degree of coherence between brain regions (obtained by averaging the eigenvalues of dFC matrices over the time points in which the respective state occurred in the interictal and ictal sessions), and correlated with reference RSNs (Yeo and Smith repertoires).

3.3.1.1. Analysis of relevant dFC states: temporal metrics and correlation with RSNs

Regarding the partition model k = 10 obtained with the AAL90 atlas and PC method, state 8 displays a statistically significant between-session difference in the mean lifetime (p-value = $5.92 * 10^{-6}$), spending longer periods in the ictal session (averaged mean lifetime ± standard error = 5.05 ± 0.46 TR) than in the interictal session (1.80 ± 0.92 TR). Furthermore, the frequency of this FC pattern is also signify-cantly higher during the ictal phase (averaged probability of occurrence ± standard error = 0.088 ± 0.023) than in the interictal phase (0.015 ± 0.009), although this metric did not pass the correction for multiple comparisons. Regarding the FC strength, state 8 presents significantly different (p-value = 0.015) eigenvalues between both sessions, with stronger FC during the ictal phase (mean eigenvalue of 56.16 ± 1.34) than in the interictal phase (52.58 ± 0.73). This FC pattern is depicted in **Fig. 7. A.**

Regarding other states for this partition model, the global mode (state 1) is the most strongly connected state regardless of the phase of the migraine cycle (higher mean eigenvalues in both sessions in comparison to the remaining states), exhibiting significantly higher FC strength (p-value < 0.05) when occurring in the interictal session (mean eigenvalue of 70.94 ± 2.61) than in the ictal session (64.36 ± 0.88).

Furthermore, state 3, which is significantly correlated with Yeo's VN and Smith's VMedN, VOccN and VLatN (p-value < 0.05/Σk), and state 7, without any significant correlation to Yeo RSNs, also reveal significantly higher FC strength (p-values < 0.05 and 0.05/k, respectively) in the ictal session than in the interictal session. The VN in state 3 is composed of regions from the occipital lobe (calcarine fis-sure, cuneus cortex, lingual gyrus, occipital superior, middle and inferior gyri); fusiform gyrus, belonging to both occipital and temporal lobes; and parietal lobe (parietal superior gyrus). (**Fig. 7. B**). Hence, results suggest that during the migraine attack, besides the higher mean lifetime and probability of occurrence of the DAN/FPN state, this network also presents stronger FC in comparison to the attack-free period. This observation is also valid for the VN (state 3), however, the differences in terms of mean lifetime and probability of occurrence did

not present statistical significance for this atlas.

Regarding the solutions of this statistical analysis for the remaining atlases, the partition models chosen to be analysed for each atlas followed the aforementioned criteria, being k = 14 for the AAL116, k = 9 for Desikan and k = 13 for Harvard-Oxford. The DAN/FPN state described for the AAL90 (state 8, k = 10) can also be found with significant between-session differences in the results obtained with the AAL116 atlas – state 10 (k = 14), significantly correlated with Yeo's DAN and FPN and Smith's left FPN (r = 0.28, 0.57 and 0.52, respectively) – and the Harvard-Oxford atlas – state 9 (k = 13), significantly correlated with Yeo's DAN and FPN and Smith's right and left FPN (r = 0.54, 0.47, 0.56 and 0.64, respectively). Regarding the Desikan atlas, state 9 (k = 9) overlaps with Yeo's FPN and Smith's left FPN (r = 0.46 and 0.46, respectively). One should note that all the correlations with RSNs passed the significance threshold corrected for the whole sample of tests performed (p-value < 0.05/Σk).

Similar to the AAL90 atlas, the DAN/FPN FC pattern presents significantly higher mean lifetime (p-value < 0.05/Σk), probability of occurrence (p-value < 0.05) and FC strength (p-value < 0.05) in the ictal session than in the interictal session for the AAL116 and Harvard-Oxford atlases. For the Desikan atlas, the FPN occurs in significantly longer continuous time periods (p-value < 0.05/k), with higher probability (p-value < 0.05/Σk) and stronger FC (p-value < 0.05) in the ictal session than in the interictal session.

Besides the DAN/FPN, other states correlated to well-established RSNs (p-value < 0.05/Σk) presented significant between-session. The global mode revealed a mean lifetime (AAL116 and Desikan, p-value < 0.05), probability of occurrence (Desikan, p-value < 0.05) and FC strength (Harvard-Oxford atlas, p-value < 0.05/k) significantly higher in the interictal session when compared to the ictal session. Regarding the VN, state 8 (Yeo's VN and Smith's VMedN, VOccN and VLatN) obtained with the AAL116 and state 5 (Yeo's VN and Smith's VMedN) obtained with the Harvard-Oxford revealed significantly higher mean lifetime and probability of occurrence (p-value < 0.05) in the ictal session than in the interictal session. Finally, with respect to the SMN, state 8 (Yeo's SMN and Smith's SMN and AudN) obtained with Desikan showed significantly higher mean lifetime and probability of occurrence (p-value < 0.05) and FC strength (p-value < 0.05/Σk) for the ictal session than the interictal session (**Fig. 7. C**). This state is composed of regions from the frontal lobe (precentral gyrus, orbitofrontal medial cortex, anterior cingulate cortex rostral, posterior cingulate cortex); parietal lobe (postcentral gyrus); paracentral gyrus, belonging to both parietal and frontal lobes; and temporal lobe (temporal superior gyrus, banks superior temporal sulcus, entorhinal cortex, temporal pole and temporal transverse cortex).

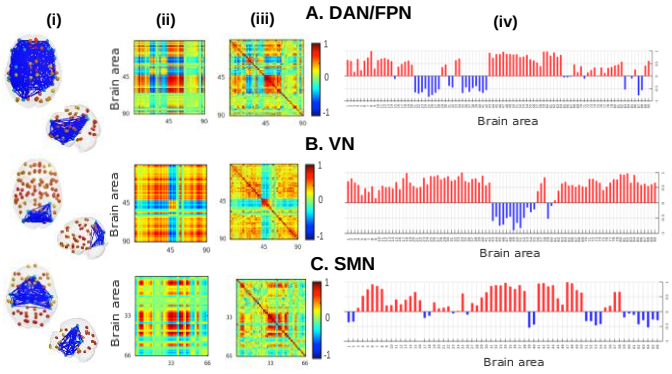

Fig. 7. States obtained with the k-means clustering algorithm (state 8, k = 10), for the AAL90 atlas (DAN/FPN state 8 and VN state 3 for k = 10) and Desikan atlas (SMN state 8 for k = 9) and with the PC method, represented by its V_c: **(i)** as a network in the atkas cortical space (axial slice), in which the elements of V_c are placed at the center of gravity of the respective brain region, shaped as spheres coloured according to their sign (red to yellow spheres represent positive elements from 1 to 0, cyan to dark blue spheres represent negative elements from 0 to -1), and areas with $V_c \leq 0.1$ are linked with dark blue edges; **(ii)** by the outer product $V_cV_c^T$; and **(iv)** as a bar plot displaying the projection of the BOLD phase in each brain region into V_c. dFC states are also characterised by their **(iii)** dFC matrix.

3.3.2. Migraineurs vs. Controls

Migraine patients scanned in the interictal phase and HC were compared by applying a permutation-based unpaired t-test on the temporal metrics of the dFC states. The *p-values* associated with the solutions obtained for the whole FC repertoire (k = 3 to k = 15) with the AAL90 atlas and PC method are displayed in **Fig. 8.**

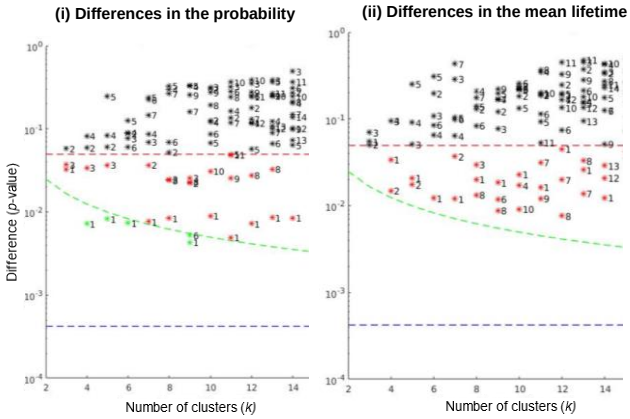

Fig. 8. Significance of between-group differences in the **(i)** probability of occurrence and **(ii)** mean lifetime of each dFC state, obtained with the AAL90 atlas and PC method, between migraine interictal session and HC, as a function of k.

3.3.2.1. Analysis of relevant dFC states: temporal metrics and correlation with RSNs

Results in **Fig. 8.** show that the global mode displays statistically significant between-group differences in the probability of occurrence and mean lifetime from k = 4 to k = 15 (0.05/Σk < p-value < 0.05) between migraine patients scanned in the interictal phase and HC. In this case, the partition model chosen to be analysed is k = 4, following the aforementioned criteria.

For k = 4, the global mode reveals a significantly higher probability of occurrence (p-value = $7.23 * 10^{-3}$), mean lifetime (p-value = $3.40 * 10^{-2}$) and FC strength (p-value = $1.40 * 10^{-3}$) in migraine patients in the interictal session compared to healthy controls. This state occurs with a probability of 0.687 ± 0.099, mean lifetime of 20.08 ± 7.08 TR, and FC strength of 67.91 ± 2.50 for migraine group, and probability of 0.391 ± 0.057, mean lifetime of 7.88 ± 0.72 TR, and FC strength of 59.63 ± 1.22 for the control group. As expected, and similarly to the behaviour observed when comparing the two phases of the migraine cycle, the global coherence state is the only FC pattern with a higher probability in migraineurs scanned in the interictal phase (in this case, compared to controls). Thus, these results suggest that, during the interictal phase, patients transit less frequently to functional networks compared to controls, spending longer continuous time periods in global mode.

Other patterns that show statistically significant between-group differences in this partition model, although not surviving multiple comparisons correction, are states 2 and 3, in which HC spend longer continuous periods of time and with higher probability than migraineurs. State 2 does not present any significant correlation with well-established RSNs, whereas state 3 is significantly correlated with Yeo's SMN and Smith's SMN and AudN. These functional subsystems are more weakly connected than the global mode.

Regarding the remaining atlases, the significant differences found in the global mode obtained with the AAL90 atlas (k = 4, state 1) can also be verified with statistical significance in the repertoires obtained with the AAL116 and Desikan (k = 5) and Harvard-Oxford (k = 4).

Furthermore, other states present statistically significant between-group differences and significant overlap with Yeo and Smith RSNs (p-value < 0.05/ Σk). In the results obtained with the AAL116 atlas, state 5 (Yeo's SMN and Smith's SMN and AudN) for k = 5 revealed significantly higher mean lifetime (p-value < 0.05) and probability of occurrence (p-value < 0.05/Σk) in migraineurs scanned in the interictal phase compared to HC. Regarding the FC repertoire obtained with the Harvard-Oxford atlas, state 4 (Yeo's VN and Smith's VMedN and VOccN) for k = 4 displayed significantly higher mean lifetime and probability of occurrence (p-value < 0.05) for patients than controls.

Although the partition models were studied following the criterium of lowest k and p-value below the most significant threshold, to observe the behaviour of the DAN/FPN network in the present comparison, the partition model k = 14 obtained with the AAL90 was analysed. For this clustering solution, it was found that state 13, which significantly (p-value < 0.05/Σk) overlaps with Yeo's DAN and FPN and Smith's right and left FPN, exhibits significantly lower mean lifetime and probability of occurrence (p-value < 0.05) in patients group than in controls.

3.3.3. Association of results with migraine pathophysiology

A summary of the results obtained in the statistical comparisons described above is displayed in **Table 1.** The stronger statistical

significance (lower *p*-value) associated with the results across atlases is registered on the table, and the labels of AAL atlas were chosen to describe the composition of the RSN detaching from the global mode.

Table 1. Summary of the results obtained with the statistical comparisons between the migraine interictal session vs. ictal session and migraine interictal session vs. HC.

FC pattern	Main findings
Global mode	**Interictal vs. Ictal** ↑ LT*, PO*, FC** **Interictal vs. HC** ↑ LT*, PO**, FC***
DAN/FPN F lobe (FIOG, IOG, OlfC, FSMedG, FMedOC, GRec, ACC, PCC); Par lobe (AnG, PrecunC); T lobe (ParaHiCG, TMG, TS and TM poles); SC regions (HiC, Amg, CdN) (AAL90)	**Interictal vs. Ictal** ↓ LT***, PO*, FC* **Interictal vs. HC** ↓ LT*, PO*
VN Occ lobe (CalFis, CunC, LinG, OccSG, OccMG, OccIG); Occ/T lobe (FusG); Par lobe (ParSG) (AAL90)	**Interictal vs. Ictal** ↓ LT*, PO*, FC* **Interictal vs. HC** ↓ LT*, PO*
SMN/AudN F lobe (PreCeG, FMG, FMOG, FIOpG, FITriG, RolOp, SuppMoA); Par/T lobes (InsC); Par lobe (PostCeG, ParSG, ParIG, SupG); Par/F lobes (ParaCe lobe); T lobe (Hechl's G, TSG, TIG); SC regions (LentNPut, LentNPal) (AAL116)	**Interictal vs. Ictal** ↓ LT*, PO*, FC*** **Interictal vs. HC** ↓ LT*, PO***

Abbreviations: A = Anterior; **Amg** = Amygdala; **An** = Angular; **C** = Cortex; **CalFis** = Calcarine Fissure; **CC** = Cingulate Cortex; **Cd(N)** = Caudate (Nucleus); **Ce** = Central; **Cun** = Cuneus; **F** = Frontal; **FC** = Functional connectivity; **Fus** = Fusiform; **G** = Gyrus; **HC** = Healthy Controls; **HiC** = Hippocampus; **I** = Inferior; **Ins** = Insular; **L** = Left; **LentN** = Lentiform Nucleus; **Lin** = Lingual; **LT** = Mean Lifetime; **M** = Middle; **Med** = Medial; **O** = Orbital; **Olf** = Olfactory; **Occ** = Occipital; **Op** = Opercular; **P** = Posterior; **Par** = Parietal; **Precun** = Precuneus; **Pal** = Pallidum; **PO** = Probability of occurrence; **Put** = Putamen; **Rec** = Rectus; **RolOp** = Rolandic Operculum; **S** = Superior; **SC** = Subcortical; **Sup** = Supramarginal; **SuppMoA** = Supplementary Motor Area; **T** = Temporal; **Tri** = Triangular; ↑/↓ = Increased/Decreased; * Significant difference before correcting for multiple comparisons (*p*-value < 0.05); ** Significant difference after correcting for multiple comparisons (*p*-value < 0.05/k); *** Significant difference after correcting for multiple comparisons (*p*-value < 0.05/Σk).

Over the past years, neuroimaging studies have revealed alterations in the functional state of migraineurs' brain compared to the normal brain condition [47], suggesting that this pathological alteration involves the sensitivity of FC to plastic and developmental changes in the functional architecture. This sensitivity may lead to the adaptation of cortical networks and reshape of functional connections to altered cognitive and emotional demands, such as chronic pain [48]. Indeed, converging evidence suggests that the increased nociceptive synaptic transmission derived from recurring headaches involves a survival pain experience that demands attention and is intimately associated with learning. Thus, the unconditioned pain stimuli may bring cognitive and sensory processing-related regions to a heightened state [49].

3.3.3.1. DAN/FPN

The DAN and FPN play an essential role in cognitive and executive processes, involving goal-directed attention, working memory, stimulus processing and perception-somesthesis-pain [44][47]. Hence, the study of dFC changes in these brain networks may provide indirect information about brain cognitive and executive integrity.

The present work results suggest that migraineurs spend longer continuous time periods, with a higher probability of occurrence and more strongly coherent brain regions, in a state composed of the DAN and FPN during the ictal phase compared to the interictal phase. The temporal metrics of this FC pattern are also higher for controls than for migraine patients in the interictal phase.

To the best of our knowledge, comparisons throughout the migraine cycle and between migraineurs and controls in terms of dynamics of FC states have not been performed so far. In contrast, FC findings have already been reported in several studies comparing these groups, although lacking consistency and reproducibility.

Regarding the DAN, Niddam et al. [50] suggest an increased sFC between the DAN and the orbital, rectal, fusiform and parahippocampal gyri, and middle temporal and occipital gyri in migraine patients in the interictal phase compared to HC. With respect to the FPN, Lee and colleagues [51] point to a decrease in the dFC of FPN, and Xue et al. [52] report an increased sFC within the frontoparietal central executive network, both in migraineurs scanned in the interictal phase compared to controls. Regarding the comparison between migraine interictal and ictal phases, literature is scarce, and as far as we are aware no statistically significant results have been published.

Converging evidence has suggested that pain and cognition systems are partially overlapped and share resources. Indeed, the "pain-cognition interactions" consist of connections between brain regions with altered activity involved in pain processing and modulation, namely amygdala, anterior cingulate cortex, middle prefrontal cortex (affective components of pain) and S1, S2, and insula (sensory components of pain), and areas belonging to the FPN that act on the cognitive control of pain (ventrolateral and dorsolateral cortices and parietal gyrus). Some of these interactions may begin before the attack but are more prevalent during the ictal phase [9][11][52].

Two main mechanisms have been hypothesized regarding the functioning of pain-cognition interactions during the attack. When simultaneously activated, pain and cognition systems may compete for resources. In those conditions, whereas healthy individuals show a mildly reduced brain activity in response to acute pain, and pain has a low ability to affect the performance of cognitive systems, migraineurs reveal a decreased cognitive task-related brain activity in response to painful stimulation [11]. This decrease can be explained by a "self-compensatory adaptation response" driven when the brain is exposed to a high sensorial load (nociceptive inputs), which induces a distraction or filtering mechanism to guarantee a less painful experience and avoid suffering [53]. Furthermore, the sole activation of pain systems (resting-state condition) is interpreted by several authors as an "additional cognitive load" that requires focused attention and management. In that case, pain enhances activity in attention-specific networks (DAN) that share resources with cognitive-related networks (FPN) [54]. Following this reasoning, it is rational to expect that, during the attack, migraineurs spend longer continuous time periods in a goal-directed attentional and cognitive state with a higher probability of occurrence and FC strength than in the attack-free period.

3.3.3.2. SMN and VN

The SMN and the VN are sensory RSNs both involved in processing external stimuli [54]. The SMN plays a vital role in action-execution motor tasks and perception-somesthesis paradigms, and the VN is associated with the visual behavioural domain, namely the processing of simple, complex emotional and high-order visual stimuli [44]. For some partition models studied, the SMN appears intermingled with the AudN, which is also integrated into the sensory system and associated with action-execution, cognition-language, and perception-audition-speech paradigms [44].

The results of this work suggest that migraineurs hold the SMN and VN for longer continuous time periods, with a higher probability of occurrence and and FC strength during the ictal phase than in the interictal phase. This behaviour of temporal metrics is also repeated for HC compared to interictal phase.

Comparing migraineurs scanned in the interictal phase with HC, Zang et al. [55] suggest an increased sFC between the left S1 and right S1, and Tu et al. [42] point to a decrease in the dFC of VN, both in the interictal session. Comparing migraine ictal and interictal sessions, Araújo [56] reports a decrease in the sFC within the SMN (somatomotor cortex), and Hougaard and colleagues [57] suggest an increase of the sFC between the visual cortex and the lower middle frontal gyrus, both for the ictal session.

One possible theory to explain the observed increased permanence and FC strength in the SMN during the ictal phase compared to the interictal phase is that the recurrent brain activation to persistent migraine attacks enhances the strength of the functional connections between brain regions involved in nociceptive processing, or in other words, it evokes the activity of pain processing networks [58]. For that matter, besides the stronger FC, it would be plausible to speculate that patients in the ictal phase spend significantly longer periods and with a higher probability in a network involved in processing pain information (SMN). Another hypothesis to support the increased permanence of migraineurs in this synchronisation pattern during the ictal phase is the "psychological manipulation" theory [59]. Studies have shown that pain experience is hugely influenced by attention and emotion, and several brain regions associated with attentional/cognitive and emotional processes also participate in pain processing. Thus, it has been suggested that psychological manipulation (e.g. distraction) can profoundly impact on our perception of pain, such does the emotional state: a positive state lowers the pain and a negative state increases the pain [59]. Hence, the attempt of migraineurs in the ictal phase to distract from pain and return to a normal state may justify its frequency in dFC states participating in attention/cognitive and pain processing systems such as in a normal brain condition (healthy subjects).

Moreover, evidence has shown that in the presence of sensory stimulation, such as visual stimuli, and pain stimulation, both inputs are sent from posterior thalamic neurons via dural and retinalthalamocortical pathways to the cortex and might affect the external sensory sensitivity in migraine patients: the perception of pain stimulation is

amplified in the presence of visual inputs, converging in an increased pain sensation, and the saliency of visual inputs is enhanced in the presence of pain [54][60]. This could explain a higher mean lifetime, probability of occurrence and FC strength of a visual processing-related network during the ictal phase of the migraine cycle compared to the interictal phase. Additionally, previous migraine studies have reported associations between enhanced sensitivity to sensory inputs and hyperactivation in brain regions involved in their processing [61]. In the present study, four of the five participants scanned in the ictal phase reported photophobia as a common symptom during the attack, which could also explain the higher permanence in the VN during the ictal phase when compared to the interictal phase.

3.3.3.3. The global mode

Results of the present work reveal that migraine patients scanned in the interictal phase spend longer periods in the global mode with a higher probability of occurrence and FC strength compared to the ictal phase and HC. Therefore, interestingly, migraineurs reveal a more similar behaviour to the HC during the attack than in the attack-free period. This effect might be associated with the habituating response deficit that occurs in migraineurs.

The habituation effect is proposed to be a cortical mechanism of protection against sensory overload, consisting of a decreased response to repeated stimuli. In patients with migraines, the repetition of sensory inputs leads, on the contrary, to a successive intensification of the response with each repetition of the stimuli, which requires a higher energy demand [11][62]. This deficit contributes to the cortical hyperexcitability and vulnerability of sensory signals in migraine.

Coppola et al. [62] report that, during the days preceding the migraine attack (interictal phase), the habituation deficit reaches its maximum, with an exaggerated habituation decrease to sensory and stress overload accompanied by increased energy demand, lower thalamo-cortical activity and thalamic control. The decreased cortical activity increased energy demand required by migraineurs in this phase of the cycle could explain its permanence in a strongly coherent state (which reflects an increased power and connectome energy [24]), and its lower probability to occur in other functional subsystems detaching from the global BOLD phase coherence (attractor states or energy landscapes characterised by local energy minima [63]) compared to the ictal phase or healthy subjects. Furthermore, sequential recordings show that, within the interval of 12 hours to 24 hours that precede the attack (preictal phase), the electrocortical patterns and energy demand tend to normalize, such as the habituation response. During the attack (ictal phase), this normalization is even more notable, so a higher tendency of migraineurs to occur in functional subsystems deviated from the global coherence state compared to the interictal period could be expected. Indeed, this is verified in the present work, since overall migraineurs present a higher mean lifetime and probability of occurrence in dFC states misaligned from the global mode in the ictal phase compared to the interictal phase (and in HC compared to migraineurs in the interictal phase). Approximately one or two days after the attack (postictal phase), the electrocortical patterns tend to destabilize again, with the increased energy demand and the deficit in the habituation response.

Therefore, these results suggest that the migraine cycle might be characterised by an increased permanence in the global mode during the interictal phase due to the habituation response deficit and an increased probability to occur in attentional/cognitive and stimulus processing-related functional networks during the attack.

4. CONCLUSION

The main goal of this work was to study dFC in the migraine brain, which is still a novel field in the literature, and compare the altered temporal properties and FC strength of the recurrent dFC states between migraineurs in the interictal and ictal phases, and between migraineurs in the interictal phase and HC, in order to infer the relation of these alterations to the disorder mechanisms and the possibility of them constituting a neuroimaging biomarker to predict migraine progression and response to treatment.

The results obtained extended previous findings and represent novel evidence to the literature, revealing that the dysfunction of migraine brain may be associated with increased temporal metrics in attentional/cognitive and stimulus processing systems during the attack, and in the global mode during in the interictal phase. Furthermore, the study of dFC corroborated evidence for the dynamic nature of the migraine brain during rest, and emphasised the suitability of this analysis to detect and assess the evolution of brain signals.

Future work regarding the study population should reproduce the analyses performed in the present study in a larger sample size, to validate the generalisability of results. Furthermore, between-group comparisons could be performed throughout the migraine cycle, by recruiting preictal and postictal patients, such as HC scanned in the corresponding menstrual phase to control for hormonal variation. Concerning the analysis, brain parcellation schemes prioritising functional homogeneity should be explored, such as group ICA, instead of atlases with sole anatomical basis that do not ensure spatial coherence within regions. Finally, to approach the inter-subject variability, the same analysis could be repeated at a subject-level, and the relationship between the obtained results and individual metrics could be studied (for example, by correlating clinical variables with the occurrence of specific states).

5. ACKNOWLEDGEMENTS

This document was written as a part of the evaluation of the MSc Thesis in Biomedical Engineering of the author at Instituto Superior Técnico. The work described herein was performed at the Evolutionary Systems and Biomedical Engineering Laboratory (LaSEEB) of Instituto Superior Técnico (Lisbon, Portugal) during the period February-October 2021, under the supervision of Professor Patrícia Margarida Piedade Figueiredo and Doctor Raquel Santos Gil-Gouveia.

BIBLIOGRAPHY

[1] R. Agosti, “Migraine Burden of Disease: From the Patient’s Experience to a Socio-Economic View,” Headache J. Head Face Pain, vol. 58, pp. 17–32, May 2018, doi: 10.1111/head.13301.

[2] C. Abbafati et al., “Global burden of 369 diseases and injuries in 204 countries and territories, 1990–2019: a systematic analysis for the Global Burden of Disease Study 2019,” Lancet, vol. 396, no. 10258, pp. 1204–1222, Oct. 2020, doi: 10.1016/S0140-6736(20)30925-9.

[3] T. J. Steiner, L. J. Stovner, R. Jensen, D. Uluduz, and Z. Katsarava, “Migraine remains second among the world’s causes of disability, and first among young women: findings from GBD2019,” Journal of Headache and Pain, vol. 21, no. 1. BioMed Central Ltd, p. 137, Dec. 01, 2020, doi: 10.1186/s10194-020-01208-0.

[4] T. J. Steiner, L. J. Stovner, T. Vos, R. Jensen, and Z. Katsarava, “Migraine is first cause of disability in under 50s: will health politicians now take notice?,” Journal of Headache and Pain, vol. 19, no. 1. Springer-Verlag Italia s.r.l., pp. 1–4, Dec. 01, 2018, doi: 10.1186/s10194-018-0846-2.

[5] F. Puledda, R. Messina, and P. J. Goadsby, “An update on migraine: current understanding and future directions,” J. Neurol., vol. 264, no. 9, pp. 2031–2039, Sep. 2017, doi: 10.1007/s00415-017-8434-y.

[6] K. P. Peng and A. May, “Migraine understood as a sensory threshold disease,” Pain, vol. 160, no. 7. Lippincott Williams and Wilkins, pp. 1494–1501, Jul. 01, 2019, doi: 10.1097/j.pain.0000000000001531.

[7] K. P. Peng and A. May, “Redefining migraine phases – a suggestion based on clinical, physiological, and functional imaging evidence,” Cephalalgia, vol. 40, no. 8, pp. 866–870, 2020, doi: 10.1177/0333102419898868.

[8] R. Burstein, R. Noseda, and D. Borsook, “Migraine: Multiple processes, complex pathophysiology,” J. Neurosci., vol. 35, no. 17, pp. 6619–6629, Apr. 2015, doi: 10.1523/JNEUROSCI.0373-15.2015.

[9] R. Gil-Gouveia, A. G. Oliveira, and I. P. Martins, “Assessment of cognitive dysfunction during migraine attacks: a systematic review,” J. Neurol. 2014 2623, vol. 262, no. 3, pp. 654–665, Dec. 2014, doi: 10.1007/S00415-014-7603-5.

[10] P. J. Goadsby, P. R. Holland, M. Martins-Oliveira, J. Hoffmann, C. Schankin, and S. Akerman, “Pathophysiology of migraine: A disorder of sensory processing,” Physiol. Rev., vol. 97, no. 2, pp. 553–622, Apr. 2017, doi: 10.1152/physrev.00034.2015.

[11] R. Gil-Gouveia and I. P. Martins, “Cognition and Cognitive Impairment in Migraine,” Curr. Pain Headache Reports 2019 2311, vol. 23, no. 11, pp. 1–10, Sep. 2019, doi: 10.1007/S11916-019-0824-7.

[12] J. Olesen et al., “The International Classification of Headache Disorders, 3rd edition (beta version),” Cephalalgia, vol. 33, no. 9, pp. 629–808, Jul. 2013, doi: 10.1177/0333102413485658.

[13] M. B. Vincent and N. Hadjikhani, “Migraine aura and related phenomena: Beyond scotomata and scintillations,” Cephalalgia, vol. 27, no. 12, pp. 1368–1377, Dec. 2007, doi: 10.1111/j.1468-2982.2007.01388.x.

[14] N. Karsan and P. J. Goadsby, “Biological insights from the premonitory symptoms of migraine,” Nature Reviews Neurology, vol. 14, no. 12. Nature Publishing Group, pp. 699–710, Dec. 01, 2018, doi: 10.1038/s41582-018-0098-4.

[15] N. J. Giffin, R. B. Lipton, S. D. Silberstein, J. Olesen, and P. J. Goadsby, “The migraine postdrome,” Neurology, vol. 87, no. 3, pp. 309–313, Jul. 2016, doi: 10.1212/WNL.0000000000002789.

[16] R. Noseda and R. Burstein, “Migraine pathophysiology: Anatomy of the trigeminovascular pathway and associated neurological symptoms, cortical spreading depression, sensitization, and modulation of pain,” Pain, vol. 154, no. SUPPL. 1, pp. 1–21, 2013, doi: 10.1016/j.pain.2013.07.021.

[17] S. Akerman, P. R. Holland, and P. J. Goadsby, “Diencephalic and

brainstem mechanisms in migraine," Nature Reviews Neuroscience, vol. 12, no. 10. pp. 570–584, Oct. 20, 2011, doi: 10.1038/nrn3057.
[18] F. M. Cutrer and J. H. Smith, "Human Studies in the Pathophysiology of Migraine: Genetics and Functional Neuroimaging," Headache J. Head Face Pain, vol. 53, no. 2, pp. 401–412, Feb. 2013, doi: 10.1111/HEAD.12024.
[19] J. M. Soares et al., "A Hitchhiker's guide to functional magnetic resonance imaging," Frontiers in Neuroscience, vol. 10. Frontiers Media S.A., p. 515, Nov. 01, 2016, doi: 10.3389/fnins.2016.00515.
[20] M. P. van den Heuvel and H. E. Hulshoff Pol, "Exploring the brain network: A review on resting-state fMRI functional connectivity," European Neuropsychopharmacology, vol. 20, no. 8. Elsevier, pp. 519–534, Aug. 01, 2010, doi: 10.1016/j.euroneuro.2010.03.008.
[21] K. A. Smitha et al., "Resting state fMRI: A review on methods in resting state connectivity analysis and resting state networks," Neuroradiology Journal, vol. 30, no. 4. SAGE Publications Inc., pp. 305–317, Aug. 01, 2017, doi: 10.1177/1971400917697342.
[22] B. T. Thomas Yeo et al., "The organization of the human cerebral cortex estimated by intrinsic functional connectivity," J. Neurophysiol., vol. 106, no. 3, pp. 1125–1165, Sep. 2011, doi: 10.1152/jn.00338.2011.
[23] M. G. Preti, T. A. Bolton, and D. Van De Ville, "The dynamic functional connectome: State-of-the-art and perspectives," Neuroimage, vol. 160, no. December, pp. 41–54, 2017, doi: 10.1016/j.neuroimage.2016.12.061.
[24] J. Vohryzek, G. Deco, B. Cessac, M. L. Kringelbach, and J. Cabral, "Ghost Attractors in Spontaneous Brain Activity: Recurrent Excursions Into Functionally-Relevant BOLD Phase-Locking States," Front. Syst. Neurosci., vol. 14, no. April, pp. 1–15, 2020, doi: 10.3389/fnsys.2020.00020.
[25] R. M. Hutchison et al., "Dynamic functional connectivity: Promise, issues, and interpretations," Neuroimage, vol. 80, pp. 360–378, Oct. 2013, doi: 10.1016/j.neuroimage.2013.05.079.
[26] S. Alonso Martínez, G. Deco, G. J. Ter Horst, and J. Cabral, "The Dynamics of Functional Brain Networks Associated With Depressive Symptoms in a Nonclinical Sample," Front. Neural Circuits, vol. 14, no. September, 2020, doi: 10.3389/fncir.2020.570583.
[27] E. Glerean, J. Salmi, J. M. Lahnakoski, I. P. Jääskeläinen, and M. Sams, "Functional Magnetic Resonance Imaging Phase Synchronization as a Measure of Dynamic Functional Connectivity," Brain Connect., vol. 2, no. 2, pp. 91–101, Apr. 2012, doi: 10.1089/brain.2011.0068.
[28] L. D. Lord et al., "Dynamical exploration of the repertoire of brain networks at rest is modulated by psilocybin," Neuroimage, vol. 199, no. May, pp. 127–142, 2019, doi: 10.1016/j.neuroimage.2019.05.060.
[29] L. H. Schulte and A. May, "Functional Neuroimaging in Migraine: Chances and Challenges," Headache, vol. 56, no. 9, pp. 1474–1481, Oct. 2016, doi: 10.1111/head.12944.
[30] S. M. Smith, "Fast robust automated brain extraction," Hum. Brain Mapp., vol. 17, no. 3, p. 143, Nov. 2002, doi: 10.1002/HBM.10062.
[31] Y. Zhang, M. Brady, and S. Smith, "Segmentation of brain MR images through a hidden Markov random field model and the expectation-maximization algorithm," IEEE Trans. Med. Imaging, vol. 20, no. 1, pp. 45–57, Jan. 2001, doi: 10.1109/42.906424.
[32] M. Jenkinson, P. Bannister, M. Brady, and S. Smith, "Improved Optimization for the Robust and Accurate Linear Registration and Motion Correction of Brain Images," Neuroimage, vol. 17, no. 2, pp. 825–841, Oct. 2002, doi: 10.1006/NIMG.2002.1132.
[33] J. Andersson, M. Jenkinson, and S. Smith, "Non-linear registration aka Spatial normalisation FMRIB Technial Report TR07JA2," 2007.
[34] L. Griffanti et al., "ICA-based artefact removal and accelerated fMRI acquisition for improved resting state network imaging," Neuroimage, vol. 95, pp. 232–247, Jul. 2014, doi: 10.1016/j.neuroimage.2014.03.034.
[35] G. Salimi-Khorshidi, G. Douaud, C. . Beckmann, M. . Glasser, L. Griffanti, and S. . Smith, "Automatic Denoising of Functional MRI Data: Combining Independent Component Analysis and Hierarchical Fusion of Classifiers," Neuroimage, vol. 90, p. 449, Apr. 2014, doi: 10.1016/J.NEUROIMAGE.2013.11.046.
[36] M. W. Woolrich, B. D. Ripley, M. Brady, and S. M. Smith, "Temporal autocorrelation in univariate linear modeling of FMRI data," Neuroimage, vol. 14, no. 6, pp. 1370–1386, 2001, doi: 10.1006/NIMG.2001.0931.
[37] S. M. Smith and J. M. Brady, "SUSAN—A New Approach to Low Level Image Processing," Int. J. Comput. Vis. 1997 231, vol. 23, no. 1, pp. 45–78, 1997, doi: 10.1023/A:1007963824710.
[38] N. Tzourio-Mazoyer et al., "Automated anatomical labeling of activations in SPM using a macroscopic anatomical parcellation of the MNI MRI single-subject brain," Neuroimage, vol. 15, no. 1, pp. 273–289, 2002, doi: 10.1006/nimg.2001.0978.
[39] R. S. Desikan et al., "An automated labeling system for subdividing the human cerebral cortex on MRI scans into gyral based regions of interest," Neuroimage, vol. 31, no. 3, pp. 968–980, 2006, doi: 10.1016/j.neuroimage.2006.01.021.
[40] J. Cabral et al., "Cognitive performance in healthy older adults relates to spontaneous switching between states of functional connectivity during rest," Sci. Rep., vol. 7, no. 1, pp. 1–13, 2017, doi: 10.1038/s41598-017-05425-7.
[41] M. H. Lee, C. D. Smyser, and J. S. Shimony, "Resting-State fMRI: A Review of Methods and Clinical Applications," doi: 10.3174/ajnr.A3263.
[42] Y. Tu et al., "Abnormal thalamocortical network dynamics in migraine," Neurology, vol. 92, no. 23, pp. 2706–2716, 2019, doi: 10.1212/WNL.0000000000007607.
[43] C. A. Figueroa et al., "Altered ability to access a clinically relevant control network in patients remitted from major depressive disorder," Hum. Brain Mapp., vol. 40, no. 9, pp. 2771–2786, 2019, doi: 10.1002/hbm.24559.
[44] S. M. Smith et al., "Correspondence of the brain's functional architecture during activation and rest," Proc. Natl. Acad. Sci. U. S. A., vol. 106, no. 31, pp. 13040–13045, Aug. 2009, doi: 10.1073/pnas.0905267106.
[45] A. Camargo, F. Azuaje, H. Wang, and H. Zheng, "Permutation-based statistical tests for multiple hypotheses," Source Code Biol. Med. 2008 31, vol. 3, no. 1, pp. 1–8, Oct. 2008, doi: 10.1186/1751-0473-3-15.
[46] A. R. Lopes, A. S. Letournel, and J. Cabral, "Altered resting-state network dynamics in Schizophrenia," medRxiv, pp. 1–9, 2020, doi: 10.1101/2020.07.21.20157347.
[47] G. Coppola et al., "Thalamo-cortical network activity during spontaneous migraine attacks," Neurology, vol. 87, no. 20, pp. 2154–2160, Nov. 2016, doi: 10.1212/WNL.0000000000003327.
[48] J. Liu et al., "Disrupted resting-state functional connectivity and its changing trend in migraine suffers," Hum. Brain Mapp., vol. 36, no. 5, pp. 1892–1907, May 2015, doi: 10.1002/hbm.22744.
[49] A. V. Apkarian, M. N. Baliki, and P. Y. Geha, "Towards a theory of chronic pain," Prog. Neurobiol., vol. 87, no. 2, p. 81, Feb. 2009, doi: 10.1016/J.PNEUROBIO.2008.09.018.
[50] D. M. Niddam, K. Lai, J. Fuh, C. N. Chuang, W. Chen, and S. Wang, "Reduced functional connectivity between salience and visual networks in migraine with aura:," https://doi.org/10.1177/0333102415583144, vol. 36, no. 1, pp. 53–66, Apr. 2015, doi: 10.1177/0333102415583144.
[51] M. J. Lee, B. Y. Park, S. Cho, H. Park, S. T. Kim, and C. S. Chung, "Dynamic functional connectivity of the migraine brain: A resting-state functional magnetic resonance imaging study," Pain, vol. 160, no. 12, pp. 2776–2786, 2019, doi: 10.1097/j.pain.0000000000001676.
[52] T. Xue et al., "Intrinsic Brain Network Abnormalities in Migraines without Aura Revealed in Resting-State fMRI," PLoS One, vol. 7, no. 12, p. e52927, Dec. 2012, doi: 10.1371/journal.pone.0052927.
[53] Z. Li et al., "The altered right frontoparietal network functional connectivity in migraine and the modulation effect of treatment:," https://doi.org/10.1177/0333102416641665, vol. 37, no. 2, pp. 161–176, Apr. 2016, doi: 10.1177/0333102416641665.
[54] Y. Zou, W. Tang, X. Qiao, and J. Li, "Aberrant modulations of static functional connectivity and dynamic functional network connectivity in chronic migraine," Quant. Imaging Med. Surg., vol. 11, no. 6, pp. 2253–2264, Jun. 2021, doi: 10.21037/qims-20-588.
[55] J. Zhang et al., "The sensorimotor network dysfunction in migraineurs without aura: a resting-state fMRI study," doi: 10.1007/s00415-017-8404-4.
[56] R. Araújo, "Functional connectivity during spontaneous migraine attacks compared to pain-free periods: a resting-state fMRI study," Master Thesis, no. November, 2020.
[57] A. Hougaard, F. M. Amin, H. B. W. Larsson, E. Rostrup, and M. Ashina, "Increased intrinsic brain connectivity between pons and somatosensory cortex during attacks of migraine with aura," Hum. Brain Mapp., vol. 38, no. 5, pp. 2635–2642, May 2017, doi: 10.1002/hbm.23548.
[58] G. Dumkrieger, C. D. Chong, K. Ross, V. Berisha, and T. J. Schwedt, "Static and dynamic functional connectivity differences between migraine and persistent post-traumatic headache: A resting-state magnetic resonance imaging study," Cephalalgia, vol. 39, no. 11, pp. 1366–1381, 2019, doi: 10.1177/0333102419847728.
[59] M. C. Bushnell, M. Čeko, and L. A. Low, "Cognitive and emotional control of pain and its disruption in chronic pain," Nat. Rev. Neurosci. 2013 147, vol. 14, no. 7, pp. 502–511, May 2013, doi: 10.1038/nrn3516.
[60] A. . Harriott and T. . Schwedt, "Migraine is Associated With Altered Processing of Sensory Stimuli," doi: 10.1007/s11916-014-0458-8.
[61] F. Puledda, D. Ffytche, O. O'Daly, and P. J. Goadsby, "Imaging the Visual Network in the Migraine Spectrum," Front. Neurol., vol. 10, Dec. 2019, doi: 10.3389/FNEUR.2019.01325.
[62] G. Coppola, F. Pierelli, and J. Schoenen, "Habituation and migraine," Neurobiol. Learn. Mem., vol. 92, no. 2, pp. 249–259, Sep. 2009, doi: 10.1016/J.NLM.2008.07.006.
[63] A. Ashourvan, S. Gu, M. G. Mattar, J. M. Vettel, and D. S. Bassett, "The energy landscape underpinning module dynamics in the human brain connectome," Neuroimage, vol. 157, pp. 364–380, Aug. 2017, doi: 10.1016/J.NEUROIMAGE.2017.05.067.